OBLATE-EARTH EFFECTS ON THE CALCULATION OF E_C DURING SPACECRAFT REENTRY

John B. Bacon[(1)], Mark J. Matney[(1)],

[(1)]NASA Johnson Space Center XI-4, 2101 NASA Pkwy. Houston TX 77058 USA john.bacon-1@nasa.gov
[(1)]NASA Johnson Space Center XI-4, 2101 NASA Pkwy. Houston TX 77058 USA mark.matney-1@nasa.gov

ABSTRACT

The bulge in the Earth at its equator has been shown [1] to lead to a clustering of natural decays biased to occur towards the equator and away from the orbit's extreme latitudes. Such clustering must be considered when predicting the Expectation of Casualty (E_c) during a natural decay because of the clustering of the human population in the same lower latitudes. This study expands upon prior work [1, 2], and formalizes the correction that must be made to the calculation of the average exposed population density as a result of this effect. Although a generic equation can be derived from this work to approximate the effects of gravitational and atmospheric perturbations on a final decay, such an equation averages certain important subtleties in achieving a best fit over all conditions. The authors recommend that direct simulation be used to calculate the true E_c for any specific entry as a more accurate method. A generic equation is provided, represented as a function of ballistic number and inclination of the entering spacecraft over the credible range of ballistic numbers.

1. BACKGROUND

In the final stages of orbital decay, the density scale height shrinks to only a few kilometers. At the same time, the rapidly-circularizing orbit encounters two effects of the oblate Earth, each of which (at moderate to high inclinations) permute the "effective altitude" to a degree comparable to or exceeding such typical scale heights. The primary influence is the elevation of the atmosphere relative to Earth's center in the equatorial regions, simply rising in lock step with the geoid. Because the Earth's radius at the equator is 21 kilometers (km) higher than at its poles, the effective density (and thus, the local deceleration) could hypothetically increase by a factor of nearly 50 at the equator relative to values at the poles under an idealized perfect circular Kepler orbit.

Simultaneously, the J2 gravitational orbit perturbation works in the opposite direction, raising the local radius of the orbit at extreme latitudes, and dropping it at the equator. There are additional J3 effects noted by Fremeaux, *et al.*, [3] which emerge as a small correction factor in the present study. Fig. 1 shows the progression of the local altitude and radius for a decaying polar orbit, and the progression in the Log_{10} of density during the decay. All values are plotted versus latitude, causing a rocking back and forth as time progresses. Clearly, the dominant nonlinear factor in the otherwise spiral decay is the physical uplift of the atmosphere into the orbit path.

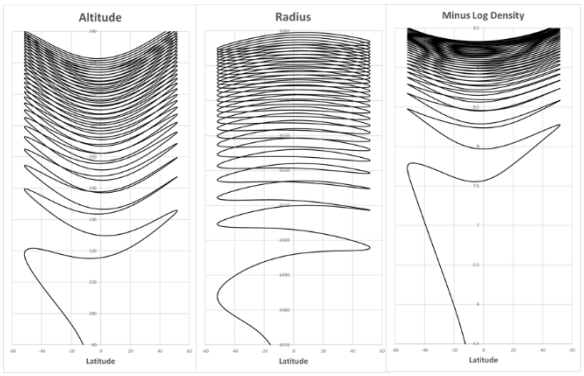

Figure 1. Altitude, radius, and Minus Log(Density) plotted vs. latitude for a decaying 50º orbit at 100kg/m2 ballistic number. While the J2 gravitational effect raises the local radius at the extreme latitudes, the elevation of the atmosphere above the physical bulge at the equator dominates the density variations encountered by the decaying spacecraft. Both the gravitational and atmospheric perturbations are evident in structure of the decay concentration curves.

With such strong cyclic variation in the drag profile, it should be expected that the distribution of natural decays around the orbit path (measured in Argument of Latitude [ArgLat with symbol Θ], which is the angle along an orbit in the orbit plane measured from the north-bound pass of the equator; generally computed as the true anomaly plus the argument of perigee) should instead show a statistical clustering that reflects this cyclic forcing function at one-half orbit period. Indeed, in earlier work, both simulation and analysis of well-documented real, natural polar orbit decays showed a cyclic clustering towards the equator. Preliminary assessments with the initial model revealed that the statistical biasing of natural decays to the more heavily populated lower latitudes could have up to a 13% effect on the calculated value of E_c. When the authors presented the preliminary model they acknowledged that further work would be necessary to completely define the statistical biases under different values of ballistic number (BN), inclination, and perhaps solar flux conditions. This paper reports the conclusion of that work, covering a full range of credible ballistic numbers

and all orbit inclinations. Solar flux was shown in subsequent publication [2] to be inconsequential to the decay latitude bias problem. In the improved model the authors have reformulated the analysis in terms of ArgLat instead of latitude, which has allowed better comparison of the physics across cases.

2. APPROACH

Tens of thousands of natural decays were simulated in the NASA General Mission Analysis Tool (GMAT), in parametric studies every 5° of inclination for spacecraft with 50, 100, 150, and 200 kg/m^2 BN decaying for slightly more than 50 orbits each. The orbits were propagated to 90 km altitude. (Past research [2] has shown that at 90 km the residual time and distance to go to the surface is approximately independent of ArgLat for any given ballistic number. Therefore, to reduce computation time from weeks to days, the decays were truncated at 90 km). This truncation must be accounted for when considering actual expectation of casualty, because ground intercept will be several degrees downrange of the calculated entry point.

GMAT is a certified NASA mission planning tool with an adaptive step, ninth order Runge-Kutta integrator with eighth order error control that can numerically integrate the path of a decaying object through a selectable atmosphere. In this study, the MSIS-E 2000 atmosphere was modeled at F(10.7) identical daily and 90-day average values of 115 janskys, and the global geomagnetic index Kp constant was uniform at 3. Orbits were propagated with 4th-order spherical harmonics and full atmospheric responses to day-of-year and the orbit's Right Ascension of the Ascending Node (RAAN).

The mass of the modeled spacecraft was dithered in tiny steps to achieve a cumulative 2% spacecraft mass variation in 101 uniform steps per run. The mass dither is considered by the authors to be the subtlest and most linear way to induce a smooth variation in a very nonlinear process. This method allows the initial conditions to be as nearly identical as possible, while allowing the forces being studied to integrate in the nonlinear ways under study. The 2% total mass variation in a decay with more than 50 remaining orbits at inception is enough to observe one full cycle of the ArgLat of decay. (One hundred and one runs are needed to generate 100 gaps. It is the gaps that drive the compression data.).

Once a full cycle of ArgLat was observed, the relative compression (or "compression factor") C(Θ) of the decays was recorded at each value of Θ. C(Θ) is calculated by talking the ratio of the spacing between the ArgLat of any one iteration's decay and the next iteration's value, divided by the averaged step size over the full 360° cycle of ArgLat. (The non-integer number of steps is linearly interpolated between integer steps that bracket the 360° cycle.) A clustering of decays in one portion of the arc then yields a ratio less than one, and a rarefaction or sparseness of decays will lead to a number greater than one. Although this may seem counterintuitive, representing a variable angle per incremental decay scenario (vs. variable decays per unit angle) was the most easily immediately-normalized function when establishing common compression curves. When the function is inverted to a probability distribution function, each local point must be binomially expanded, as discussed later.

> *Example*: if 57.137 uniform increments of a satellite's mass caused the decay's ArgLat to vary by 360°, the average step size would be (360°/57.137) = 6.2751°. If the argument of decay latitude shifted only 5.72° from one iteration to the next at a particular region, the local compression rate would be (5.72°/6.2751) = 0.9115°

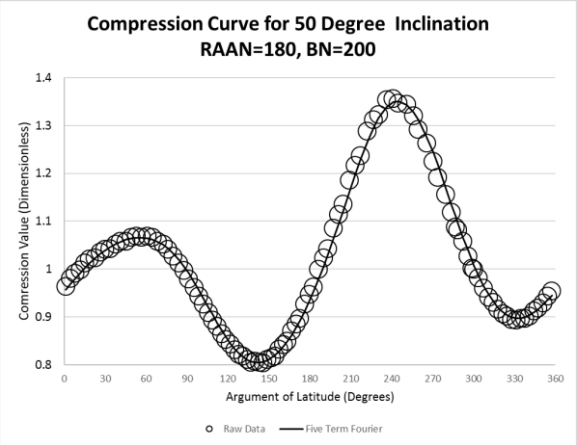

Figure 2. An example relative compression curve for BN=200 decays at 50° inclination and RAAN=180°. The curve illustrates the excellent fit of the five-term Fourier approximation. At the vernal equinox, this orbit has a beta angle of zero and passes directly under the subsolar point, creating a day-night asymmetry in the decay rate. The near mirror of this curve occurs at 90° RAAN (see Fig 6). The asymmetry is removed by plotting the rates at four orthogonal RAANs and averaging the curves. (This is best done after curve-fitting, because there is no way to align the individual statistical points to achieve the same values of ArgLat in all four plots.) Note in the curve how sparse the entry events are at the peaks relative to the valleys, in terms of spatial density of the points.

The resulting plot of relative compression vs. ArgLat shows a consistent cyclic behavior of concentrating entries as the decay location approaches the equator (ArgLat= 0 and 180), receding rapidly after passing it, and becoming most rarefied approaching the extreme latitudes (ArgLat = 90 and 270). An example plot is shown in Fig. 2. A 5-term Fourier analysis of the data is

superimposed as the solid line, showing an excellent fit, with generally <0.7% average error of the fit from recorded values. The universal model of the compression curve over all conditions is generated by characterizing the trend of the first four best-fit Fourier coefficients under varying ballistic number, RAAN, and inclination. (The fifth term represents residual noise, but no implicit physics emerges from its trending.) Noise comparable to or greater than the fifth Fourier amplitude coefficient is introduced in the estimation of the curve in 256 discreet bins of ArgLat with nearest value in the true compression curve.

The entire series was repeated at four orthogonal orbit planes (RAAN=0, 90, 180, and 270) at the vernal equinox. The reason for RAAN variation was to average out the effects of the diurnal variation in the atmosphere, which presents variations in density of up to 25% of peak value, depending upon whether Θ lies near the terminator, subsolar point, or solar midnight.

In all then, (4 ballistic numbers) × (4 RAANs) × (101 runs/case) × (18 inclinations) led to 29,088 sample runs, leading to 288 curves of 100 data points each. An additional 30 special cases were run to explore conditions at the solstice, simplified gravitational models, and extreme ballistic numbers, for yet another 3030 runs.

Next, all 100 compression data pairs for each set of input conditions were spread into the closest of 256 uniform ArgLat bins. A Fourier analysis was performed on this 256-bin representation of the curve. The amplitude and phase of the first five oscillating terms were recorded, with the first term (the uniform average compression) defined as being one despite any curve-fitting residual.

The five Fourier terms were then explored for empirical trends, such that the amplitude and phase of each term can be derived for any input. The empirical formulation of the Fourier terms then, in theory, allows us to recreate the compression curve for any condition. Ultimately, chaotic trends in the phases of asymmetric Fourier terms, and low-inclination orbits in general were problematic to developing a fully-universal empirical prediction.

From the relative compression C(Θ) along such a reconstituted curve we can derive the relative likelihood of impacting at any particular latitude. For any given inclination (i) and ArgLat (Θ), we get that the latitude is ARCSIN(SIN(i)*SIN(Θ)), and the local statistical likelihood at that latitude relative to unit average will be a binomial expansion of 1/C. The coefficient 1/C must be binomially expanded to achieve the original true compression in relative decays per degree. This problem stems from the mathematical inequality that the most easily normalized initial compression curve is based upon N/Avg(X), which is not equal to N*Avg(1/X).

3. RESULTS

Each compression curve takes the general form of a sinusoidal curve in (two times the) ArgLat, (a 2Θ harmonic), perturbed by 1Θ, 3Θ, and 4Θ harmonic terms of generally lower amplitude, each term affected by a unique phase offset.

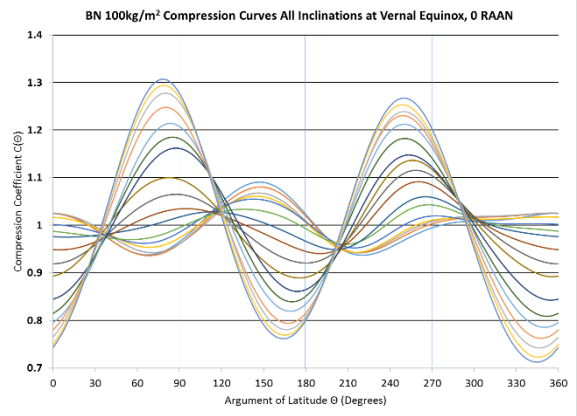

Figure 3. A family of compression curves for inclinations from 5° to 90° at RAAN=0° and BN=100 kg/m². Curve amplitude near 90° ArgLat increases with orbit inclination. The curves are more chaotic and invert the compression effect's locations at the lower inclinations, although at low amplitude and low inclination, the net effect on latitude clustering is small.

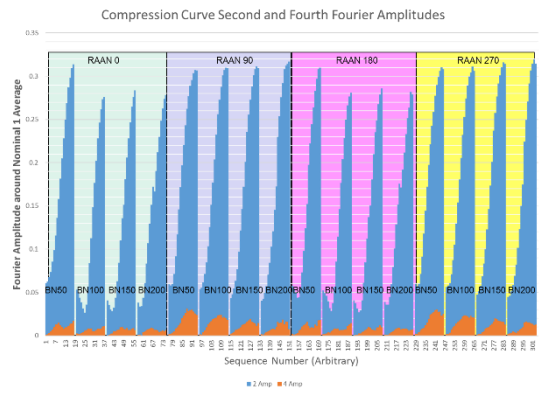

Figure 4a. The even-numbered (symmetric) Fourier term amplitudes of compression curves. Note that the 2Θ terms are typically a factor of 10 larger than the 4Θ terms and the patterns generally repeat with comparatively small variations for ballistic number and RAAN. In each of the 16 tooth-shaped curves, orbit inclination increases from 5 at the left to 90° at the right. Each of four major groupings shows the results for one RAAN value: 0°, 90°, 180°, and 270° from left to right. Within each group, each of four ballistic numbers are evaluated: 50, 100, 150, and 200 kg/m².

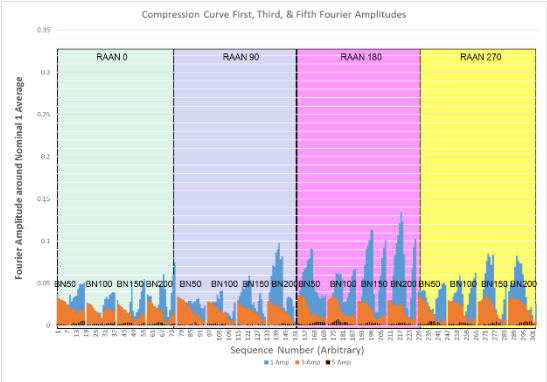

Figure 4b. The odd (asymmetric) Fourier term amplitudes of the compression curves. The groupings are as in Fig. 4a, and the vertical axis is to the same scale. The simple first harmonic wave in Θ is the largest but most irregular of all the secondary terms, and is believed to be heavily influenced by the exact path through or near the subsolar point, potentially containing some J3 gravitational information too. Note the interesting and as yet unexplained gap in most 1Θ amplitudes near 50°-55°. The 3Θ terms are very repeatable and are likely purely atmospheric in nature (see Fig 5c). The 5Θ terms are completely negligible, representing noise. (The gravitational model itself is only to four harmonic terms.)

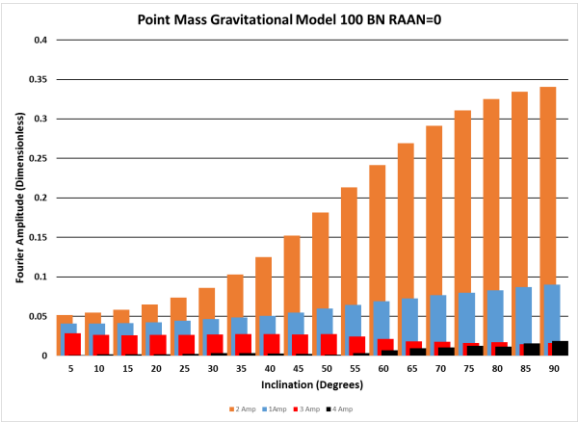

Figure 5a. The scale of atmospheric vs. gravitational effects is evident in the calculation of compression curves when Earth's simple point-mass gravitational model (0-order, 0-degree gravitational model) is used instead of the full 4-order, 4-degree gravitational model. Only atmospheric geometry—especially the solar heating effect—is driving the Θ, 3Θ, and 4Θ Fourier terms in this case, resulting in perturbing effects generally comparable in scale with the "wall of air" effect at low inclinations, dropping to about 25% influence at the highest inclinations for the 1Θ term, and <5% influence for the higher-order terms.

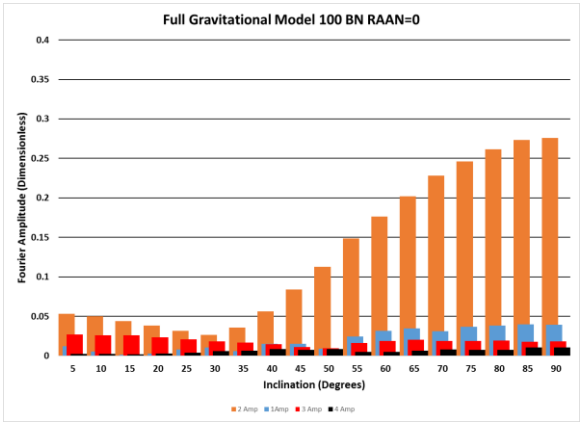

Figure 5b. The compression curve Fourier coefficients when the full gravitational model is used for the same conditions of 100 kg/m2 ballistic number and 0° RAAN. Note the reduction in nearly all of the coefficients, indicating that gravitational forces in many cases may mitigate the atmospheric effects.

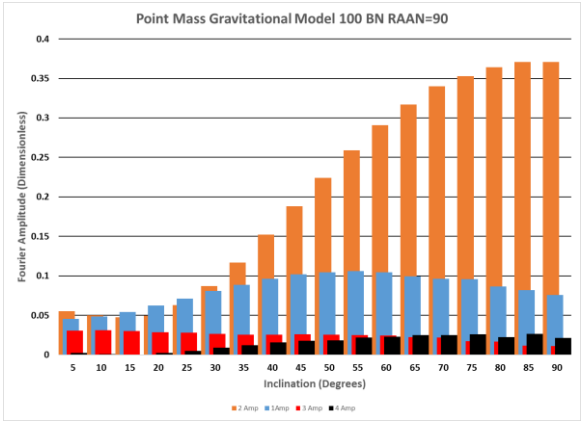

Figure 5c. The point mass gravitational model for a 100 kg/m^2 BN at 90° RAAN. Note the shift in height and shape of the 1Θ (blue) term, and the increase in the 2Θ (orange) term, all presumably due to atmospheric effects only. The path of the orbit relative to the subsolar point has a noticeable effect on the symmetry of the curve (Fig. 6). Note that the 3Θ (red) term is remarkably consistent across all the curves. This strongly implies that the J3 terms are atmospheric in nature, and real.

The basic 2Θ curve has an uprange offset of 15°-20° relative to nodal crossings at 0° and 180° of ArgLat at higher inclinations, with interesting trends in the opposite direction at the lower inclinations, where all the Fourier terms have comparable amplitudes. The shape of the curve is generally more disorganized at lower inclination orbits, but still exhibits this basic behavior (see Fig. 3).

The first five Fourier terms' amplitudes are shown in Figs. 4a and 4b grouped into terms that are respectively even and odd multiples of Θ, representing the effects that are symmetric north-to-south and those that are asymmetric.

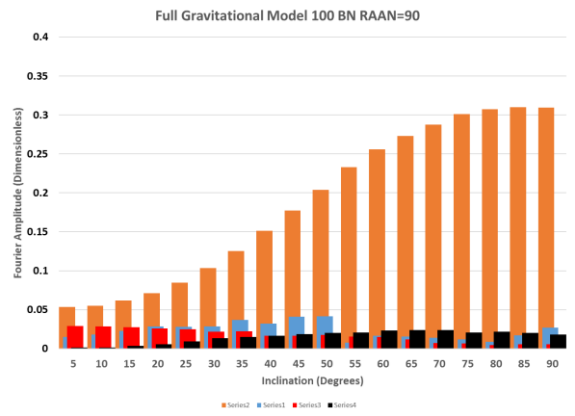

Figure 5d. The same conditions as in Fig. 5c above, with the full gravitational model employed. As with the RAAN=0 case pair, most Fourier terms have been reduced from the point-mass gravity model's case.

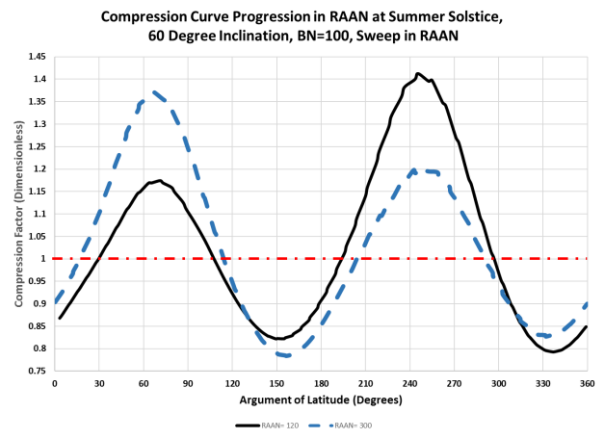

Figure 6a. The compression curve changes in character with passage of the orbit near the subsolar point at the summer solstice. Here a 60° inclination orbit of 100 kg/m2 ballistic number was propagated every 15° in RAAN, ultimately lining up nearly through maximum density a few degrees east of the subsolar point when the initial RAAN at the start of the propagation was 120°. At RAAN = 300° (+180° of RAAN from 120°), the curve family reached a nearly mirrored amplitude profile. It illustrates the effect on symmetry of major perturbing effects in the atmosphere other than the equatorial bulge that causes the basic SIN(2Θ) curve. When all 22 runs are sequenced, the curves exhibit a simple harmonic "sloshing" with cycling RAAN.

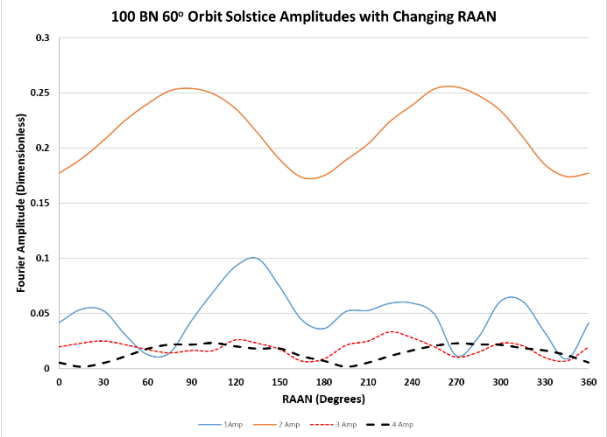

Figure 6b. The variation in Fourier term amplitudes with RAAN for the sweep of a 60° orbit. Note that the 2Θ amplitude term peaks well before the full compression curve does.

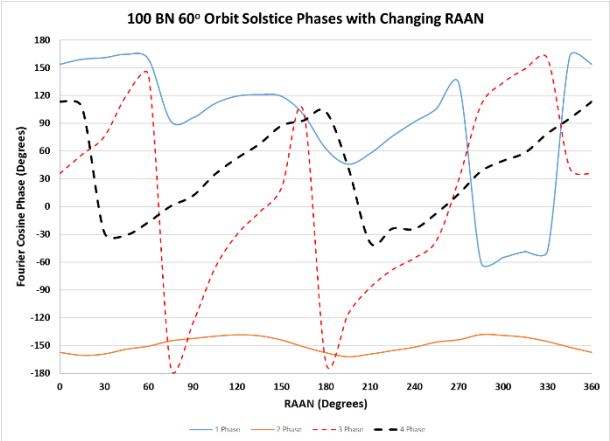

Figure 6c. The variation in Fourier term phases with RAAN for the sweep of a 60° orbit.

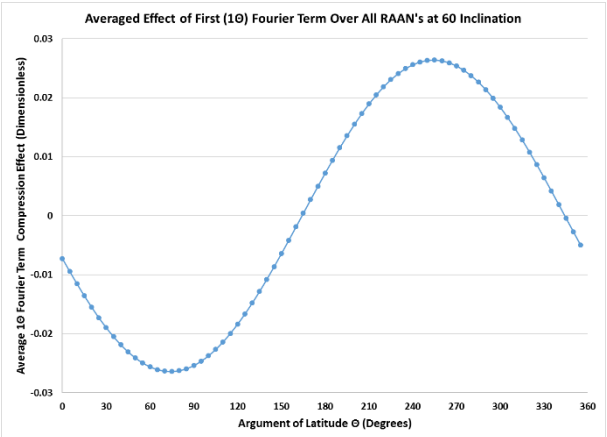

Figure 6d. When the first Fourier term in 1Θ is averaged at each value of Θ over all RAANs, a perfect sine wave emerges, representing the residue believed to be the J3 gravitational contribution. This slightly biases natural decays to occur in the northern (vastly more populated) hemisphere.

From the Fourier amplitudes in Fig. 1 (especially in the 90° and 270° RAAN cases) there is an apparent increasing trend in the peak 2Θ Fourier amplitude with increasing ballistic number. A special series of high ballistic number cases was run to explore this trend, with the peak amplitude at 90° inclination plotted in Fig. 7. From this we derive there is a simple quadratic trend in the symmetric compression effect as a function of ballistic number, while the asymmetric effects are increasingly less significant.

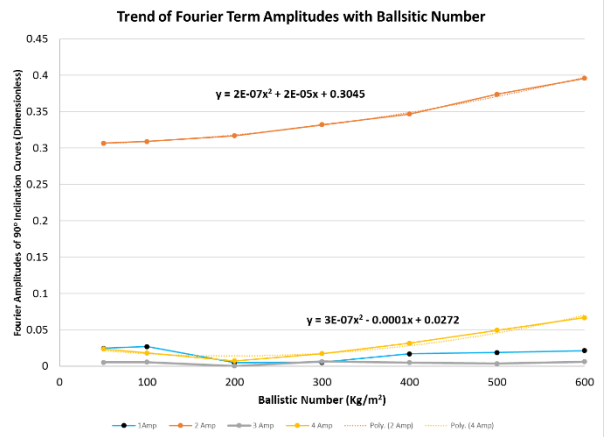

Figure 7. The trend of the first four Fourier term amplitudes for peak inclination orbits as ballistic number increases. The symmetric first and fourth terms show a simple quadratic growth, while the odd terms remain flat and comparatively small.

It should be noted that it is only the symmetric terms that progress monotonically in phase, while the asymmetric terms present a less ordered structure (see Figs. 8 and 9).

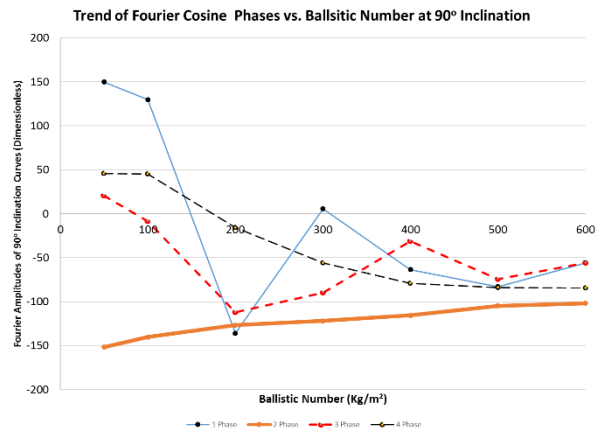

Figure 8. The phases of the 2Θ and 4Θ Fourier (cosine) terms are the only monotonically changing curves in the significant components of the compression curves.

The phases of the Fourier terms generally show a much noisier trend as a function of orbit inclination than do the amplitudes. A set of phases for one set of inclinations under common RAAN and BN conditions is shown in Fig. 9. As we have mentioned earlier, the compression curves do not exhibit particularly strong predictable structure in the lower inclinations. As in the high-ballistic-number study, only the even-numbered (symmetric) terms show a monotonic and convergent behavior with increasing inclination.

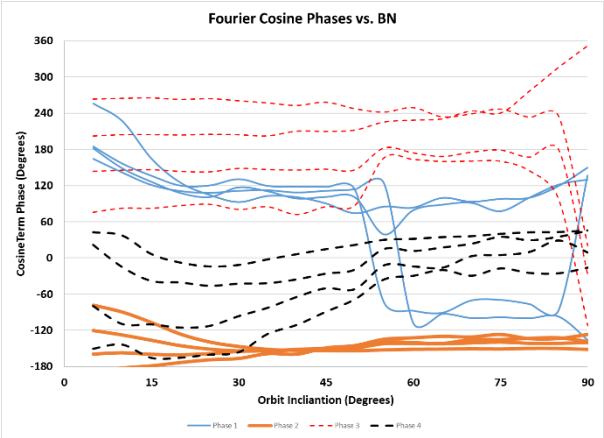

Figure 9. The phases of the first four cosine terms of the compression curves for all ballistic numbers at 90° RAAN. There are four curves for each Fourier phase term: one for each ballistic number (50, 100, 150, and 200 kg/m^2). The curve for each successively higher ballistic number initiates farther lower on the graph than it did for the prior (smaller) ballistic number. Note the erratic behaviour of the asymmetric terms. (Phase 1 and Phase 3, implying the offsets from ArgLat = 0° of the 1Θ & 3Θ cosine terms.) The jump appears coincident in inclination with the gap in the amplitude trend, evident in Fig. 4b). Only the 2Θ family is very well behaved over all inclinations.

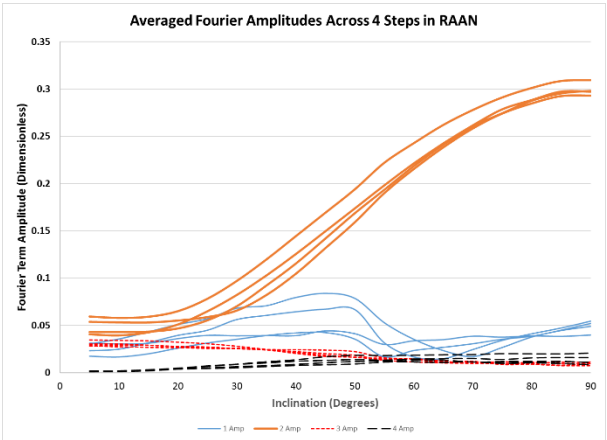

Figure 10. The amplitudes of the first four Fourier terms of the compression curves, each averaged across four orthogonal RAANs. As with Fig. 9, each of four parallel curves starts lower than the curve for the next lower ballistic number.

4. DISCUSSION

The physics of decay biasing are difficult to discern empirically in highly nonlinear and interacting gravitational and atmospheric density domains that are each modelled with many orders of comparable-scale and often competing perturbations. Even the 30,000+ simulations of the current study are insufficient to isolate all the pure physics, although some key effects are emerging.

The authors propose that the first four Fourier terms are sufficiently well-behaved in amplitude and phase that they can be used to generate a representative compression curve for any selected ballistic number and orbit inclination. The most problematic of these is the 1Θ term, which as seen in Fig. 6d is likely harboring real J3 gravitational effects observed by Fremeaux, *et al.* [3] along with the diurnal atmosphere effects. While the diurnal effects are large, these should be averaged out when estimating expectation of casualty for decays sufficiently far in the future that specific dates and RAANs are completely unknown.

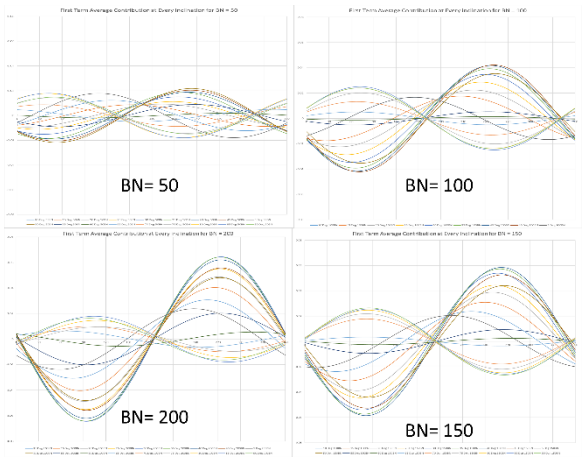

Figure 11. The average of the first Fourier term over four orthogonal RAANs at every value of ArgLat reveals a family of regular sine curves similar to that seen in Fig. 6d, whose amplitude and general regularity both grow with ballistic number. Each curve is a different inclination orbit, and all four plots are to the same scale. The curve amplitudes peak near 40° inclination and invert at the highest inclinations, but generally indicate a small preference (0.06 peak, vs 0.35 peak value in the two terms) to enter in the Northern Hemisphere for most orbits.

Although only four RAAN's were explored at the equinox (vs. the 22 at the solstice for one inclination shown in Figs. 6a-6d) the data can be similarly averaged to reveal (with some inherent noise) that the J3 effect seen in Fig. 6d is clearly at work. Fig. 11 is a compilation of the residue (average) curves of the 1Θ term as a function of ArgLat at the equinox for each of four ballistic numbers 50, 100, 150, and 200, clockwise from upper left.

The 3Θ phase term is sufficiently well behaved across all ballistic numbers and all inclinations below 85°, and its amplitude sufficiently small that it should be included, although its phase seems to be problematic. As evidenced by the point-mass gravitational study illustrated in Figs 5a-5d, the 3Θ term is expected to be atmospheric in nature. Fortunately, where the phase becomes noisy and suspect, the amplitude of the correction falls to near zero (perhaps an initial reason for the noise in estimating phase).

4.1 The Model

The authors continue to refine the model and the general understanding of the latitude biasing phenomenon in natural decays. The data presented has been used to build an ***approximate*** model of the compression curve for any set of conditions (see below). However, the cumulative errors in curve-fitting and then interpolating each Fourier term indicate that the most precise answer for any planned decay will be to perform a full simulation for the exact ballistic number and inclination of the vehicle in question, averaged over a continuum of RAANs (*i.e.*, every 15°) on a date near the equinox. This does not take long using the analytical tools developed for this study.

The next best model is to linearly interpolate the 8 Fourier coefficients in phase and amplitude for any given ballistic number and inclination between the available 288 data sets. This model is what will actually be rolled into screening software and quick-study tools, as it is a tabular lookup that can run well in a spreadsheet. This method takes many thousands of data elements that cannot be presented easily in a publication, and which will be under ongoing update and refinement.

The expedient, but least accurate approximate model presented here is an empirical derivation that—while far from perfect—is substantially more accurate than the prior assumption of a fully random decay along the ArgLat, and is useful for broad parametric studies to determine peak areas of concern in calculating E_c. This model uses a set of "eyeball fit" empirical curves to model the change in coefficients.

The model is built as follows:
Each Fourier term F_N of Nth order has an Amplitude A_N and a phase offset Φ_N to create a term of the form:

$$F_N = A_N * Cos\,(N*\Theta + \Phi_N)$$

In the equations that follow, ***BN*** is the ballistic number in kg/m^2, and ***INC*** is the inclination of the orbit in degrees.

a) $F_0=A_0=1$

b) The first Fourier term represents the averaged first-term contributions over all RAANs for any given ballistic number. The resulting average is expected to be the effect of J3 gravitational perturbation as the principal 1Θ driver into the nonlinear atmosphere. Until further simulations reveal more detail, the evident simplest trend from the preliminary 4-RAAN average is a family of curves with the same phase:
   a. The amplitude of the first Fourier Term is estimated as the empirical fit: $A_1=.0418+.000125*\mathbf{BN}*Sin((5.86*\mathbf{INC})+227°)$
      i. Note: the amplitude goes negative
   b. $\Phi_1 = 0°$
      i. *for low* ***BN***
      $\Phi_1 = 100°*sin(2*\mathbf{INC}+40°)$
      ii. *for BN >50*

c) The dominant second term F_2 follows a $\sin^3$ fit to inclination:
   a. $A_2= .0498 +0 .2576*sin^3(\mathbf{INC})$
   b. $\Phi_2 = 192°*\mathbf{BN} -170$
      i. *for INC >45°*
      $\Phi_2 = 70°*\mathbf{BN}$
      i. *for INC <45°*

d) The F_3 and F_4 terms should most correctly be estimated from the averaged curves in all RAANs. This work has not been completed, and will be better done once a broader set of RAANs have been studied. The two terms are estimated from trend data at all four RAANs as follows:
   F_3:
   a. $A_3= .0334 -.0003*\mathbf{INC}$
   b. $\Phi_3 =(\mathbf{BN})^{0.85}-60°$

e) The F_4 term follows
   a. $A_4=.0206-(8.5E-7)*(400-\mathbf{BN})*\mathbf{INC}$
      i. *for* ***INC*** $< 55°$
      $A_4=0.0206-(4.683E-5)*\mathbf{BN}$
      ii. *for* ***INC*** $>55°$
   b. $\Phi_4 =130 - 0.78*\mathbf{BN} + (\mathbf{BN}/50)*(\mathbf{INC}-50°)$
      i. *for* ***INC*** $< 55°$
      $\Phi_4 = (135-\mathbf{BN}/8)-\mathbf{INC}$
      i. *for* ***INC*** $> 55°$

The fits of these respective parametric representations to the averaged Fourier terms is illustrated in Fig. 12.

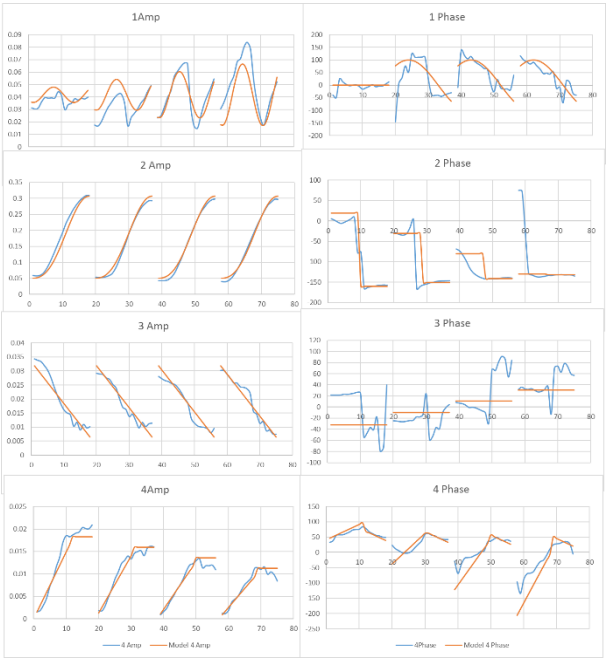

Figure 12. The empirical fits described in this section to the Fourier coefficients for compression curves at each inclination, averaged across four orthogonal RAANs at the Vernal Equinox. The four curves in each plot represent the coefficients for the four studied ballistic numbers in ascending order left to right. The jumps in the 2Θ and 3Θ phase curves do not lend themselves to simple models, and reconstructed curves in the regions of these breaks can show obvious qualitative differences.

Two representative fits of the empirical curve to the averaged scenario and to representative original simulation data are shown in Figs. 13a and 13b for orbits not situated within 5° of a break point in the empirical curve sets.

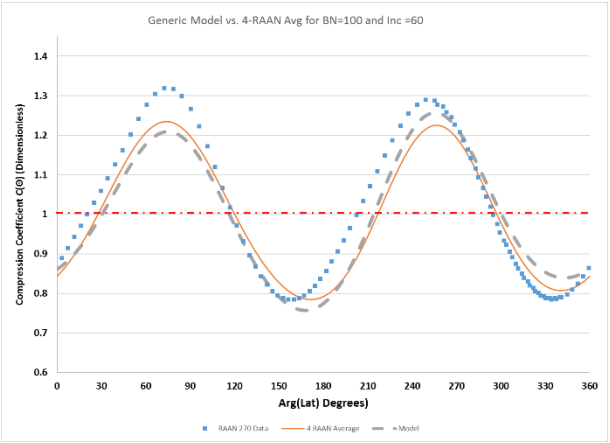

Figure 13a. Empirical (dashed) fit to the 4-RAAN average (solid) model for moderate BN and inclination. Data trace (points) from 270° RAAN is included to demonstrate how actual conditions will typically vary from the average on any given day.

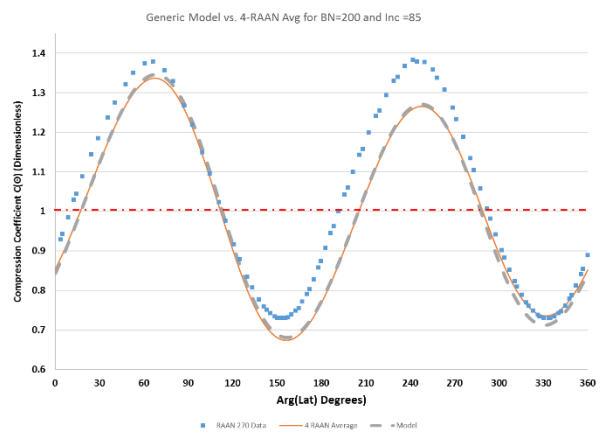

Figure 13b. The same comparison for high BN and inclination. The fit to the 4-RAAN average is excellent, but the statistical noise for any particular day of entry (in the form of the diurnal variation) is more evident.

4.2 Final E_c Calculation

With the averaged concentration factor available at each latitude, the E_c for a particular decay can finally be calculated with a slight modification to the traditional approach. The ArgLat at 90 km is incremented in small steps from 0° to 360°. The concentration factor is calculated for the ArgLat at 90 km for the specific orbit inclination and spacecraft ballistic number. A necessary pad of a few degrees is added to the ArgLat (variable with the ballistic number of the object in question) to propagate the debris farther downrange to the ground. (The calculation of this pad is beyond the scope of this paper.) The physical latitude on the planet associated with the adjusted impact ArgLat (Θ_{impact}) is calculated by the simple equation:

$$Latitude = ARCSIN(SIN(INC)*SIN(\Theta_{impact})) \quad (1)$$

The population in any given latitude band is extracted from the gridded population of the world, with a model of population growth applied. In the critical adjustment, this population is divided by the concentration factor associated with the 90-km ArgLat Θ to give an adjusted risk. The binomial correction that must be applied to correct for a normalized Probability Function is $P=(1/C(\Theta))-(1-C(\Theta))^2$. Note that the impact latitude will be encountered twice during this process (ascending and descending), with a different concentration factor applied. Each incremental risk is multiplied by the size of the incremental step in ArgLat divided by 360°, such that the sum of all steps is the total risk over the orbit.

The resulting mean population per square kilometer can be mapped as a function of inclination and ballistic number, as shown in Fig. 14, illustrating the difference in resulting risk under the new model, compared to the prior randomized-entry assumption. Expectation of casualty is a linear multiple of the mean exposed population per square kilometer, scaling as well with Debris Casualty Area. The ratio of the average populations under various inclination orbits is a weak function of ballistic number, as shown in Fig. 15.

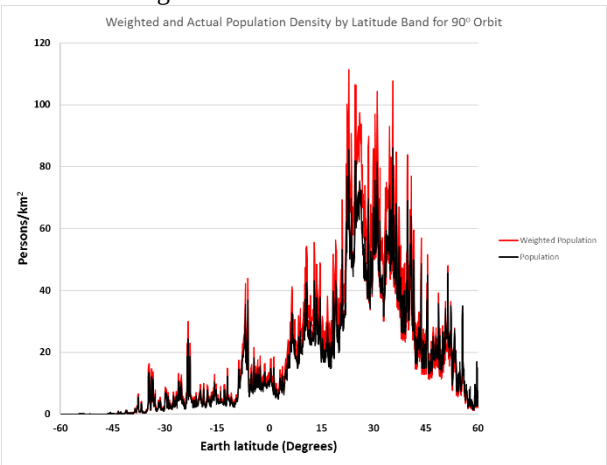

Figure 14. Weighted vs unweighted 2020 population under a 90° orbit

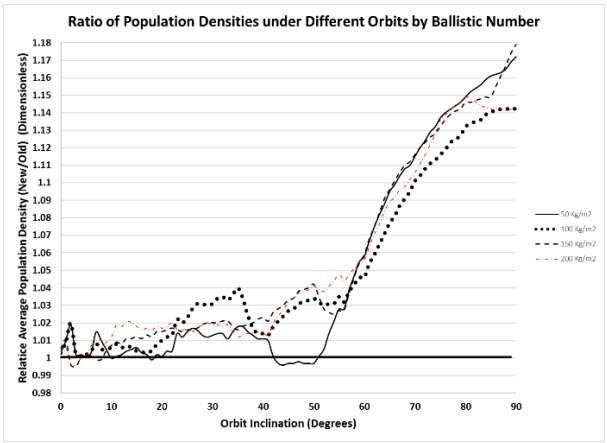

Figure 15. Ratio of mean population density under compression curve vs. the assumption of uniform decay around the orbit, as a function of orbit inclination for four ballistic numbers. A Θ_{impact} of 13.5 degrees downrange after the 90km altitude is included in this calculation.

4.3 Comparison with Prior Models

Prior work [1] identified a sinusoidal perturbation of the decay probability as a function of latitude, and implied a full symmetry of the effect. On an average case, this is approximately true, but for any particular orbit, the present work now shows the decay to be statistically clustered more strongly on the *approach* to the equator, as explained above. The physics of this has been discussed in [2], and there are significant ramifications for exceptionally low-dV intentional tactical de-orbit scenarios. In natural decays which usually occur over an indeterminate, broad timescale, many of these subtleties

largely average out, but still have influence on the entry statistics.

In the current work, the representation has been shifted to a function of *Argument* of latitude, and not latitude, to achieve a more universal formulation, and to search for underlying physics. The current work also recognizes and accommodates remaining asymmetries in statistical decays, and refines the model for ballistic number differences.

The prior method of estimating E_c incorporated a rudimentary concentration factor based upon how long a circular orbit dwells over any given latitude. Typically, this correction is applied symmetrically around the equator in an algorithm to adjust the latitude-averaged population bands in strips only a few tens of kilometres wide to account for this circular "dwell time". In the method described within this paper, this correction is not applied independently, substituting instead a localized concentration factor in tiny numeric integration steps in ArgLat, applied and integrated band by band. Note that the prior method actually places stronger likelihood of decay at the latitude extremes, and minimizes the effect at the equator, in complete opposition to the effect explored here. The effective weighting of population is evident in Fig. 14.

To conclude the forward work described in the authors prior study [1], the influence of F(10.7) solar flux variations was shown in [2] to be negligible in the critical final eight orbits when the decay rate is geometrically increasing. This is because the expansion of the atmosphere results from radiant energy deposited above the altitudes where the lowest density scale heights (and thus, maximum effect of perturbations) occur.

Conversely, the global geomagnetic index (Kp) was shown to be the driving factor to disturb low altitude atmospheric density. Geomagnetic index (updated every 3 hours) determines the energy deposition of charged particles in the altitudes driving the final few orbits of decay. From a statistical standpoint, the Kp variation is rapid and random enough to only add noise to the more consistent geodetic effects of the wall of air and of J2 perturbations. That said, the effect of Kp is significant when attempting a drag-centric targeted decay on any particular day.

5. CONCLUSIONS

The statistical clustering of natural decays towards the equator has been reduced to an approximate parametric representation accounting for ballistic number, inclination, and gravitational perturbations, useful for parametric studies and potentially for insight into the physics. Some of the corrections to prior practice can lead to localized E_c changes of up to 36% over the random-decay assumption, and net integrated E_c's that are 18% or more different than prior practice would estimate. There is strong evidence that a slight bias of natural decays occurs in the northern hemisphere due to the J3 gravitational effect.

However, the chaotic nature of some parameters indicates that best precision will come from a dedicated simulation of each decay's ballistic number and orbit inclination (and especially, if known, the date and range of likely RAANs for the expected decay), rather than the inherently "fuzzy" approximation to the specific case in a set of global parameters that seek to optimally fit a broader range of cases.

The clustering is most conveniently rendered as a function of the ArgLat, which can then be transformed to latitude. With the local compression factor available, it is a minor adjustment to existing look-up tools to generate a statistically-weighted E_c that accounts not only for the inhomogeneity in the population density with latitude, but as well for the inhomogeneity in the distribution of decays around the orbit.

6. REFERENCES

1. Bacon, J.B. & Matney, M.J. (2016). *Statistical Issues for Calculating Reentry Hazards*, IAASS 8th Workshop on Space Safety, May 21 2016.

2. Bacon, J.B (2017). *Minimum dV for Targeted Spacecraft Disposal* Proc. 7th European Conference on Space Debris, Darmstadt, Germany, 18–21 April 2017 (http://spacedebris2017.sdo.esoc.esa.int)

3. Cid Borobia, E., Fremeaux, C., and Goester J.F.: *Fast Re-Entry Deorbitation with Acceptable Risk Level* Proc. 7th European Conference on Space Debris, Darmstadt, Germany, 18–21 April 2017 (http://spacedebris2017.sdo.esoc.esa.int)